Constant Raindrop Fall Speed Profiles Derived from Doppler Radar Data Analyses for Steady Nonconvective Precipitation

ROBERT NISSEN,* ROLAND LIST, DAVID HUDAK,+ AND GREG M. MCFARQUHAR#

Department of Physics, University of Toronto, Toronto, Ontario, Canada

R. PAUL LAWSON

SPEC Incorporated, Boulder, Colorado

N. P. TUNG, S. K. SOO, AND T. S. KANG

Malaysian Meteorological Service, Petaling Jaya, Malaysia

(Manuscript received 4 January 2004, in final form 7 July 2004)

ABSTRACT

For nonconvective, steady light rain with rain rates <5 mm h^{-1} the mean Doppler velocity of raindrop spectra was found to be constant below the melting band, when the drop-free fall speed was adjusted for pressure. The Doppler radar–weighted raindrop diameters varied from case to case from 1.5 to 2.5 mm while rain rates changed from 1.2 to 2.9 mm h^{-1}. Significant changes of advected velocity moments were observed over periods of 4 min.

These findings were corroborated by three independent systems: a Doppler radar for establishing vertical air speed and mean terminal drop speeds [using extended Velocity Azimuth Display (EVAD) analyses], a Joss–Waldvogel disdrometer at the ground, and a Particle Measuring System (PMS) 2-DP probe flown on an aircraft. These measurements were supported by data from upper-air soundings. The reason why inferred raindrop spectra do not change with height is the negligible interaction rate between raindrops at low rain rates. At low rain rates, numerical box models of drop collisions strongly support this interpretation. It was found that increasing characteristic drop diameters are correlated with increasing rain rates.

1. Introduction

The variation in raindrop size distributions (RSDs) with space and time can provide important insights into rain evolution. For applications in meteorology and hydrology it is desirable to know the RSDs since they determine the radar reflectivity factor. The Marshall–Palmer (1948) distribution is such an attempt to link rain rate to radar reflectivity. The problem is that the rain rate is measured on the ground, whereas radar reflectivities are measured aloft. The use of Doppler radar, however, allows the measurement of the vertical speed distribution of the scatterers (raindrops), which can be related to the strongly diameter-dependent raindrop fall speeds. Some Doppler radar methods, which have been developed to infer RSDs remotely, will be discussed below. In this study radar signatures of RSD variations in the vertical are analyzed. Comparisons are also made with results obtained by numerical modeling of raindrop evolution by collisions and breakup.

By pointing a Doppler radar straight up, horizontal motion components disappear and radial speeds now consist of the sum of particle terminal speed, V_T, and vertical air speed, w_a. Under Rayleigh scattering, the normalized signal power density S_n at a frequency corresponding to $(w_a - V_T)$ is related to the particle diameter D, the number concentration per diameter interval, $N(D)$, and the radar reflectivity factor Z (e.g., Doviak and Zrnić 1984):

$$S_n(w_a - V_T)\, dV_T = D^6\, N(D)\, dD\, Z^{-1}. \qquad (1)$$

* Current affiliation: Environment Canada, Pacific and Yukon Region, Meteorological Service of Canada, Vancouver Office, Vancouver, British Columbia, Canada.

+ Current affiliation: Meteorological Service of Canada, King City, Ontario, Canada.

Current affiliation: Department of Atmospheric Sciences, University of Illinois at Urbana–Champaign, Urbana, Illinois.

Corresponding author address: Dr. Robert Nissen, Environment Canada, Pacific and Yukon Region, Meteorological Service of Canada, 201–401 Burrard Street, Vancouver, BC V6C 3S5, Canada.
E-mail: robert.nissen@ec.gc.ca

© 2005 American Meteorological Society

Unauthenticated | Downloaded 12/08/22 09:02 PM UTC

Early work by Probert-Jones and Harper (1961), Caton (1966), and Battan and Theiss (1966) assumed that the minimum-size drops detectable by radar corresponded to fall speeds of approximately 1 m s^{-1}. But Atlas et al. (1973) pointed out problems with this assumption such as noise-level sensitivity and the failure of small drop detection when there are disproportionately many large drops as a result of gravitational sorting. Spectra may also be broadened by turbulence (Atlas 1964). More success was achieved by Rogers (1964) using the Doppler mean velocity $\langle v \rangle$:

$$\langle v \rangle \equiv \frac{\int_0^\infty vZ'(v)\,dv}{\int_0^\infty Z'(v)\,dv}, \tag{2}$$

where Z' is the reflectivity factor per velocity interval dv. The constant spectral shape for equilibrium distributions, as discussed by List et al. (1987) would imply no variation of $\langle v \rangle$ with Z.

Assuming a semilogarithmic (Marshall–Palmer) spectrum and a simple terminal velocity–drop diameter relation of the form $V_T = aD^b$, Rogers (1964) derived a simple relation between an expected velocity $\langle v \rangle$ and Z, with the difference from measured velocity attributed to vertical air motions. Atlas et al. (1973) provided a refined fit. However, this method is still sensitive to the variations in the concentrations of the smallest drops, especially for low reflectivities.

Perhaps the most promising method today consists of the Doppler spectra measurement with height, followed by an automatic shifting of the power spectra into optimal position for assessing the air updraft speed (Thomson and List 1996). Some studies have used vertically pointed Doppler radars with longer wavelengths. Thereby Bragg scattering, which acts as a tracer for larger-scale vertical air motions, is more prominent at longer wavelengths (33 cm), with a wavelength λ dependence of $\lambda^{-1/3}$ compared to λ^{-4} for raindrops (Gossard and Strauch 1983). Larger antennas and beamwidths are used to detect the weaker backscatter at these wavelengths; however, this introduces spectral broadening due to cross-shear flow, especially with strong horizontal winds. Also, Gossard et al. (1990) found that above the cloud base, the Bragg scattering returns are usually overpowered by cloud droplets.

All strategies involving vertically pointing radar are constrained by small sample volumes, even with larger beamwidths. Although lacking full-spectrum capabilities, plan position indicator (PPI) scanning may be employed under certain conditions to obtain more precise vertical fall speeds. Seliga and Bringi (1976) introduced concepts based on orthogonal polarization analyses, with the differential reflectivity $Z_{\rm DR}$ (in dB) defined as

$$Z_{\rm DR} = 10 \log\left(\frac{Z_h}{Z_v}\right), \tag{3}$$

where Z_h and Z_v are the radar reflectivity factors derived from horizontal and vertical polarizations, respectively. Larger drops have higher $Z_{\rm DR}$ values when viewed at low elevation angles. However, there is still a lack of experimental data to validate shapes of freely falling raindrops at lower pressures.

The approach used in this investigation originates with the velocity azimuth display (VAD) analyses, as developed by Lhermitte and Atlas (1961). The radial velocity V_R of a falling precipitation particle is given by

$$V_R = (u \sin\beta + v \cos\beta)\cos\alpha + W_P \sin\alpha, \tag{4}$$

where β is the azimuth angle measured clockwise from north, α is the elevation angle, and u, v, and W_P are the eastward, northward, and upward components of particle motion, respectively. A horizontally linear wind field is assumed with particle fall speeds W_P varying only in the vertical. These assumptions are best satisfied during steady-state stratiform precipitation events, and can be tested by plotting derived wind velocities in a holographic representation as a function of height for different elevation angles (Figs. 1a–1c). In steady-state conditions the plots will be highly consistent with no changes of W_P being horizontally advected. For a ring of data at a constant range and low elevation, the fit of the radial velocity variation with the azimuth can be made

$$V_R = a_0 + a_1 \sin\beta + b_1 \cos\beta. \tag{5}$$

The divergence of the horizontal wind $\nabla \cdot \mathbf{U}_H$ can then be obtained from

$$a_0 = \nabla \cdot \mathbf{U}_{\rm H} \frac{r\cos\alpha}{2} + W_P \sin\alpha, \tag{6}$$

where r is the radius of the VAD circle. Figures 2a and 2b give representations of radial speeds from two different elevation angles but at the same height. It is evident that the a_0 term is dominated by particle fall speeds at high elevation angles [both r and $\cos\alpha$ decreasing in Eq. (6)] whereas divergence is more prominent at low elevation angles. The extended VAD (EVAD) algorithm was developed by Srivastava et al. (1986). For a given height interval, Eq. (6) is applied to several elevation angles. Plotting of $[2a_0/(r\cos\alpha)]$ versus $[(2\tan\alpha)/r]$ yields a slope of W_P and an intercept of $\nabla \cdot \mathbf{U}_H$. The validity of the assumptions can be assessed from the scatter of the fit. The vertical airspeeds w_a are extracted by integrating the inelastic continuity equation:

$$\rho_{\rm a} \nabla \cdot \mathbf{U}_{\rm H} + \frac{\partial(\rho_a w_a)}{\partial z} = 0, \tag{7}$$

where ρ_a is the air density and z the height above ground. The Doppler mean terminal velocity can then be obtained from

$$V_T = w_a - W_P. \tag{8}$$

Profiles of fall speeds representative of the larger drops

Unauthenticated | Downloaded 12/08/22 09:02 PM UTC

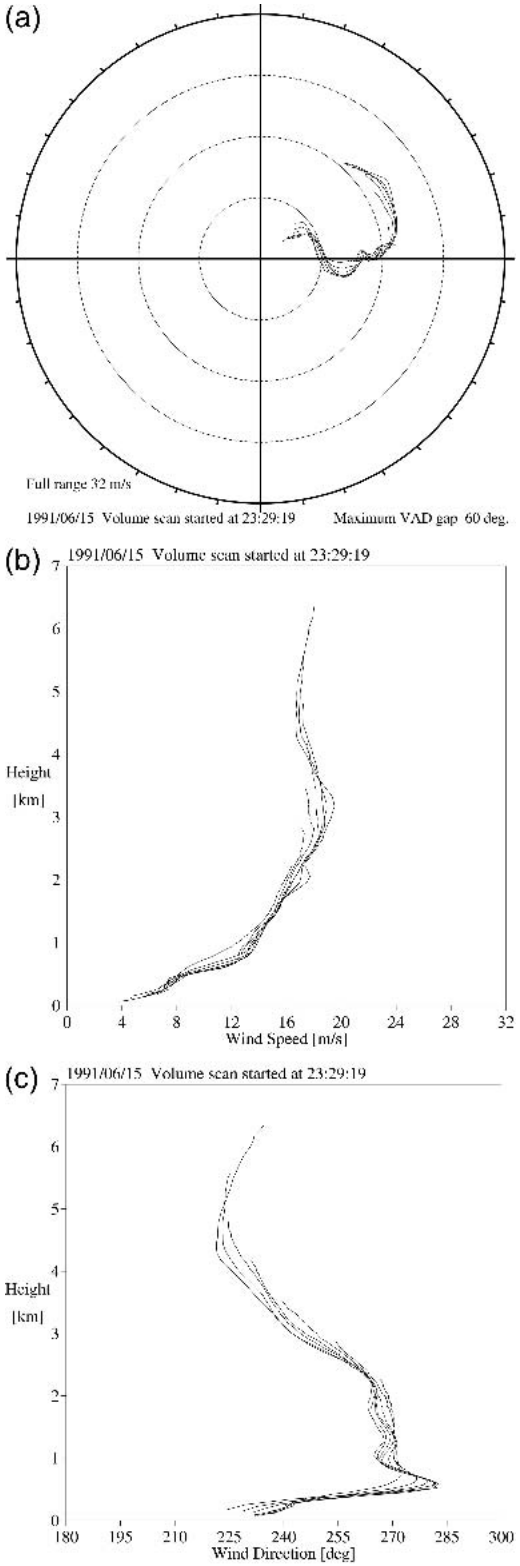

FIG. 1. A sample VAD evaluation of horizontal winds for Doppler radar data taken at 15 elevation angles ranging from 5° to 75°. Each line represents one elevation angle: (a) hodograph representation, (b) wind speed profile, and (c) wind direction profile.

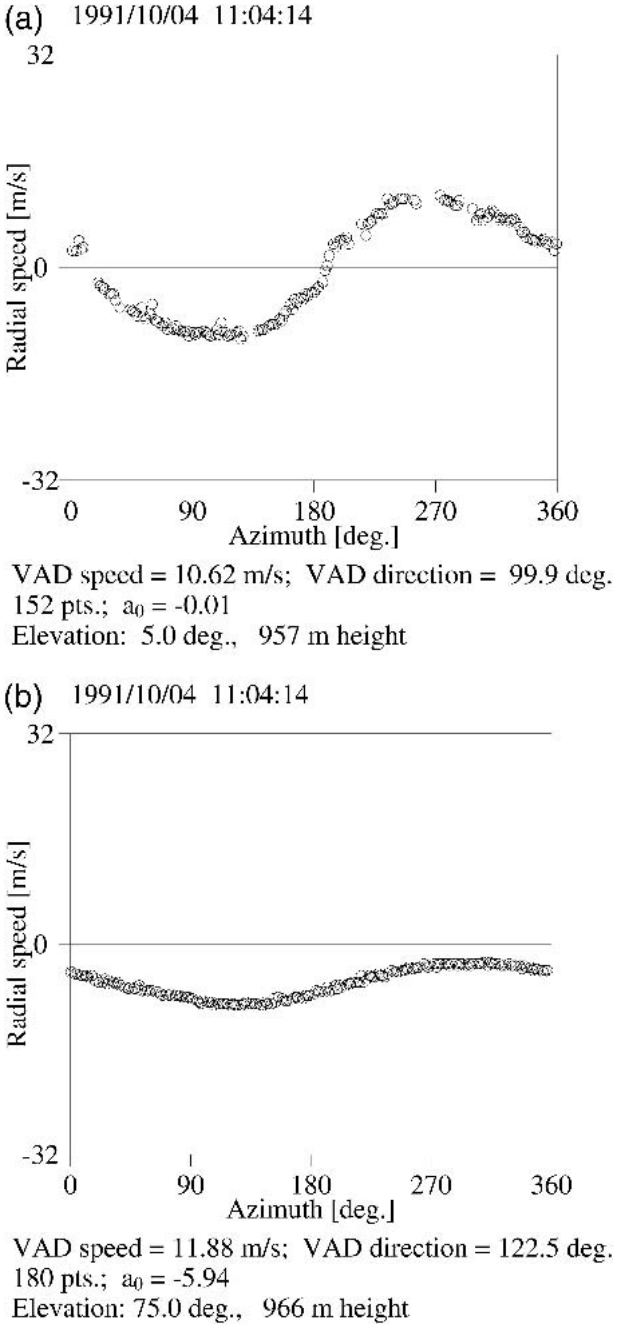

FIG. 2. A sample VAD representation of Doppler radar data taken at constant range for elevation angles of (a) 5° and (b) 75°.

can be calculated. Matejka and Srivastava (1991) further refined the EVAD method with weighing factors.

2. Implementation

Radar data were obtained with the University of Toronto X-band Doppler radar. This portable unit has an effective beamwidth of 2.5° and an antenna measuring 0.90 m in diameter. Pulse widths are either 1.0 or 0.4 μs, the latter allowing a pulse repetition frequency

Unauthenticated | Downloaded 12/08/22 09:02 PM UTC

(PRF) of 2000 Hz and a corresponding Nyquist velocity of 16 m s^{-1}. Staggered (interlaced) PRFs extended the unambiguous velocity to 32 m s^{-1} for a 3:2 ratio of PRFs, and to 48 m s^{-1} for a 4:3 ratio of PRFs. Maximum range resolution is 125 m. Four primary moments could be collected: uncorrected reflectivity, corrected reflectivity (zero radial velocity component of spectra removed), velocity, and spectral width. Values are digitized to 8 bits per moment for each range bin. Thus, reflectivity values are rounded to the nearest 0.50 dBZ, and velocities to the nearest 0.125 m s^{-1} (0.375 m s^{-1} when using a 4:3 PRF ratio) are available at the highest PRF. The radar can also be operated in a vertically pointing configuration. The computer program ASCOPE can acquire full spectrum information for each range gate with a cycle time of the order of 1 min depending upon task parameters.

At all times ground measurements for RSDs were provided by a disdrometer of the type described in Joss and Waldvogel (1967). The instrument was modified to measure time and electrical signal for each single-drop impact. The measuring area is 50 cm^2, with surrounding acoustic foam minimizing rain splash. Data are acquired with a time resolution of 1 s, and are binned into 1024 diameter channels ranging from 0.16 to 5.2 mm. However, the smallest drops recorded measure about 0.25 mm in light rain, with a deterioration of the lower threshold to 1.0 mm in heavy rain. The calibration followed that of McFarquhar and List (1993) to eliminate uneven operation of amplifiers. A plot of diameter versus time for each drop was used to identify periods of steady, mainly stratiform rain. The Doppler mean velocity $\langle v \rangle$ was determined from time-averaged RSDs using Eqs. (1) and (2).

One dataset was collected in Penang, Malaysia, (5°12′N, 100°18′E, elevation 4 m) during the Joint Warm Rain Experiment of the Malaysian Meteorological Service and the University of Toronto, which ran from 25 September to 8 November 1990. The radar was located at Bayan Lepas Airport in the southeast portion of Penang Island, 4 km from the shoreline. Hills with elevations up to 800 m high, 5 km to the northwest contribute ground clutter for radar scans up to 7° elevation. The disdrometer was located less than 50 m from the radar, and the upper-air soundings were launched from the airport grounds.

The other dataset was collected at the University of Toronto, Canada, (43°40′N, 79°24′W, elevation 174 m) from late March to early November 1991, with both the radar and the disdrometer on top of the Physics building 60 m above ground level. The nearest sounding sites were Buffalo, New York, and Flint, Michigan.

3. Results

a. Penang, 2 November 1990

For this case, in situ measurements by the King Air research aircraft of the Malaysia Meteorological Service provided another check of the precipitation particle spectra with a Particle Measuring Systems (PMS) 2-DP probe (effective diameter range 0.6 to 6.4 mm). Auxiliary data were provided by two Rosemount probes, one for air temperature, the other for static air pressure (Rosemount 1201 Altitude Transducer). The temperature versus pressure variation among the Rosemount probes was in excellent agreement with sounding data, thus the height above ground could be determined. Although the inertial navigation system was not functional, horizontal distance relative to the radar was calculated using a combination of event makers enacted whenever the aircraft was over the radar, together with airspeed deduced from dynamic pressure measurements. For the 2-DP probe data, images with embedded blank slices were rejected. The "center-in" option was used; that is, if an end diode in the first or last slice was occluded, then at least one other diode in that slice would need to be occluded for the image to be accepted. Thus, the 2-DP sample dimensions were 0.64 cm across and 26.7 cm along the laser beam. Figure 3 displays some sample images.

Doppler radar data were obtained for an elevation angle of 70.0°, while reflectivity data only were recorded for 63.6°, 54.5°, and 41.0°. As mentioned in the discussion of Fig. 2, the second term on the right-hand side of Eq. (6) is much larger than the first term at high elevation angles. Thus, the particle fall speed W_P may be obtained from the simplification $W_P = a_0/\sin\alpha$.

Figure 4 shows the fall speed profile from the radar data taken at 1844 local time (LT; UTC + 8 h). The top of the melting layer is at about 4.8 km, with fall speeds increasing to faster values just below. A fall speed profile, calculated using the pressure-dependent equations of Beard (1976), is superimposed for a drop of 2.0-mm diameter. It is evident from the radar data that no drop speed evolution takes place below the melting layer because no significant change is observed in fall speeds other than that due to changes in air pressure. Similar trends have been noted by other researchers. For example, Cifelli et al. (2000) concluded no significant size changes were taking place for profiler-retrieved parameters taken in stratiform regions of mesoscale convective systems at Darwin, Australia.

For the disdrometer data, the period of steady rain from 1840 to 1850 LT (see Fig. 5) was used to calculate the mean drop size spectrum. The derived mean fall speed is denoted by the open circle in Fig. 4. There is good agreement with the derived values from the radar data analysis when this profile is extrapolated from 1-km height down to the ground. The actual radar-derived profile near the ground is affected by ground clutter.

The aircraft passed directly over the radar site at 1846:10 LT. Flight elevation was 1640 ± 10 m and the ground speed 82 m s^{-1} (85 m s^{-1} airspeed with a southwesterly head wind speed of 3 m s^{-1} as determined by VAD analysis of Doppler radar data). The period from

Unauthenticated | Downloaded 12/08/22 09:02 PM UTC

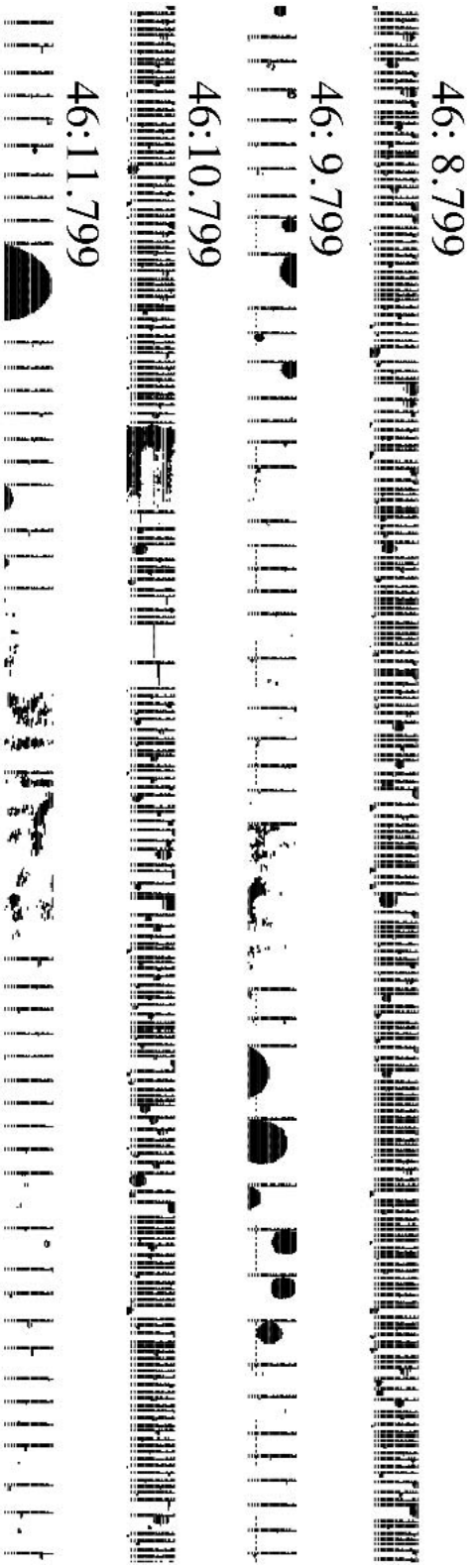

FIG. 3. Sample images from the aircraft-mounted PMS 2D probes. The first and third lines are from the 2-DP probe and the other two lines are from the 2-DC probe. Time bars separate images. Nondrop images are instrument artifacts.

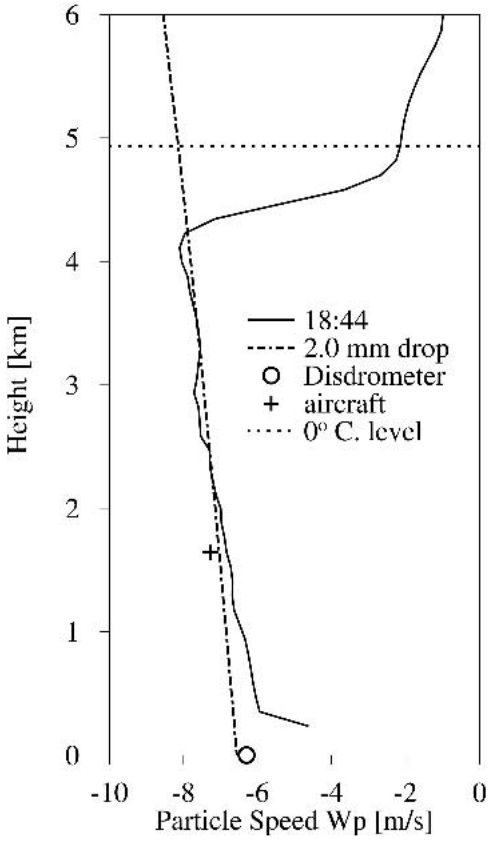

FIG. 4. Particle fall speeds derived from Doppler radar data acquired at an elevation angle of 70° (solid line) beginning at 1844 LT on 2 Nov 1990. The dash–dot line is the fall speed profile for a raindrop of 2.0-mm diameter. The "+" indicates the height and derived fall speed value for raindrop spectra measured by the aircraft 2-DP probe. The "○" indicates the derived fall value for the raindrop spectra measured by the disdrometer. For this and subsequent figures all nonradar fall speeds are calculated using the equations of Beard (1976).

1846:03 to 1846:17 LT was chosen to correspond with that of the aircraft's transit through the radar PPI scan at 70° to give a sample length of 1150 m. A total of 172 acceptable drop images were recorded by the 2-DP probe. A Doppler mean velocity was derived from this drop size spectrum incorporating aircraft-measured pressure and temperature in the fall speed determination. This velocity is indicated by the "+" symbol in Fig. 4, and is in good agreement with the radar-derived profile at this level. Increasing the sample time of the 2-DP data from 14 to 60 s results in an increase in the derived fall speed by only 0.3 m s^{-1}.

Figure 6 shows the evolution of the fall-speed profiles for successive volume scans. The shifting of the profiles with time is largely related to advection. Variations in the source at the top (pulses) would result in profile anomalies progressively propagating to lower levels on the order of 10 min. For the 1837 LT scan, larger drops have not yet been horizontally advected over the radar

Unauthenticated | Downloaded 12/08/22 09:02 PM UTC

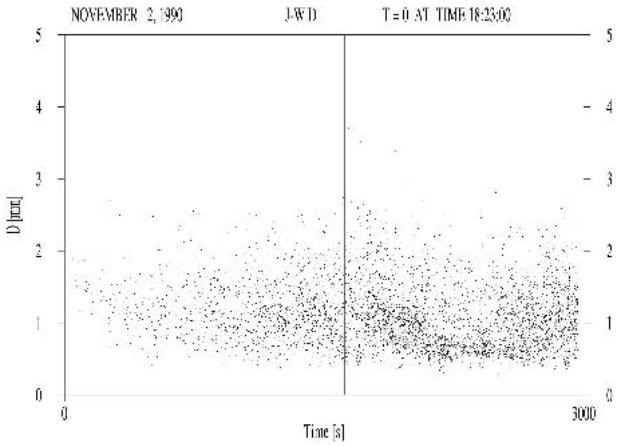

FIG. 5. Disdrometer data for the period 1823–1913 LT on 2 Nov 1990. Each dot represents a drop, indicated by its diameter, impacting at the indicated time. The vertical lines highlight the period 1840–1850 LT from which the average derived fall speed value is calculated for Fig. 4.

at low levels, but subsequent scans show better temporal consistency. This further supports the argument of very little drop size evolution below the melting layer. Reflectivity data support the advection-related trends in raindrop fall speed values.

b. Penang, 25 October 1990

On this day, radar data were recorded, chronologically, at 62.0°, 50.6°, 34.7°, and 17.0° in a "modified constant altitude PPI (CAPPI)" task (McFarquhar et al. 1996; List et al. 1991), where successive PPIs in a scanning cycle approximately follow the precipitation downward. The drop fall speed profile taken at 1944 LT from the volume scan below the melting layer (Fig. 7) is very consistent with the fall speed of a raindrop of 2.3-mm diameter. However, upward vertical airspeeds derived by EVAD analyses were 0.3 to 0.7 m s^{-1}. When these vertical airspeeds are removed from the profile, there is better agreement with the free fall speed profile of a raindrop of 2.5-mm diameter. These fall speeds are faster than those for the 2 November case. The conditions were locally stratiform but some thunderstorm activity occurred upwind. It is evident that conditions favored growth of snowflakes with large mass that then melted into large raindrops. Stronger reflectivities above the melting layer compared to the 2 November case are also consistent with the presence of ice particles with greater mass. As with the previous case, the radar-derived profile near the ground is affected by ground clutter.

The disdrometer data indicated that steady rain fell from 1949 to 1957 LT. Thus, this period was chosen to calculate a derived fall speed, which is indicated with an open circle in Fig. 7. There is good agreement with the fall speed profile from the radar data. There is better agreement with the fall speed profile from a 2.5-mm-diameter raindrop. In Fig. 8, fall speed profiles for successive radar scans are shown to be similar to Fig. 6. Just below the melting layer, fall speeds are anomalously large compared to the profile farther below. This feature is not an artifact of the analysis, but persists, developing at 1936 and continuing until 1952 LT. It is apparent that some snowflakes of very large mass are melting into large raindrops that are more vulnerable to breakup in collisions with smaller drops. Once this initial adjustment to the drop spectra has occurred, further evolution is much slower and not even detectable. On 2 November (Fig. 6), when emerging raindrops are smaller, no anomalously large fall speeds were observed at the bottom of the melting layer.

c. Toronto, 15 June 1991

Fairly steady rain fell a few hours after intense convection. The melting level was at about 4.5 km, similar in height to that commonly occurring in Penang, Malaysia. Sounding data from the upper-air station at Flint, Michigan (42°58′N, 83°45′W, elevation 233 m), was used in the EVAD analysis as the Buffalo sounding

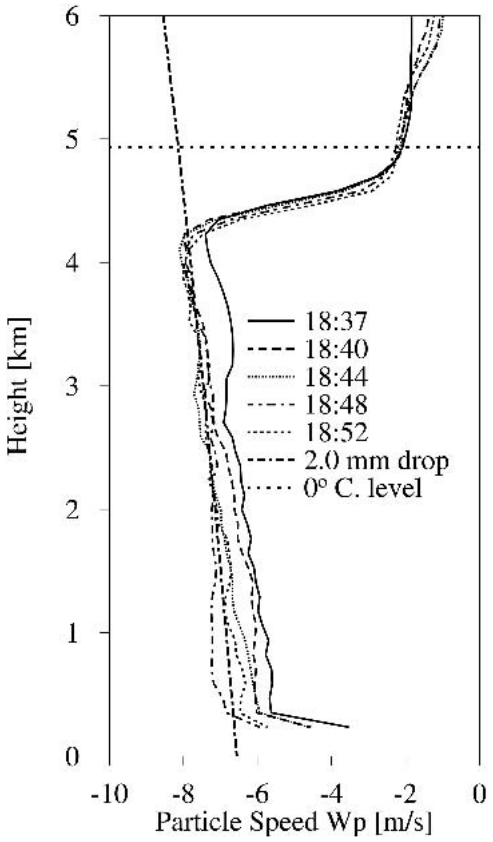

FIG. 6. Similar to Fig. 4 but for radar scans beginning at 1837 (solid), 1840 (dash), 1844 (dot), 1848 (dot–dash), and 1852 LT (short dash) on 2 Nov 1990.

Unauthenticated | Downloaded 12/08/22 09:02 PM UTC

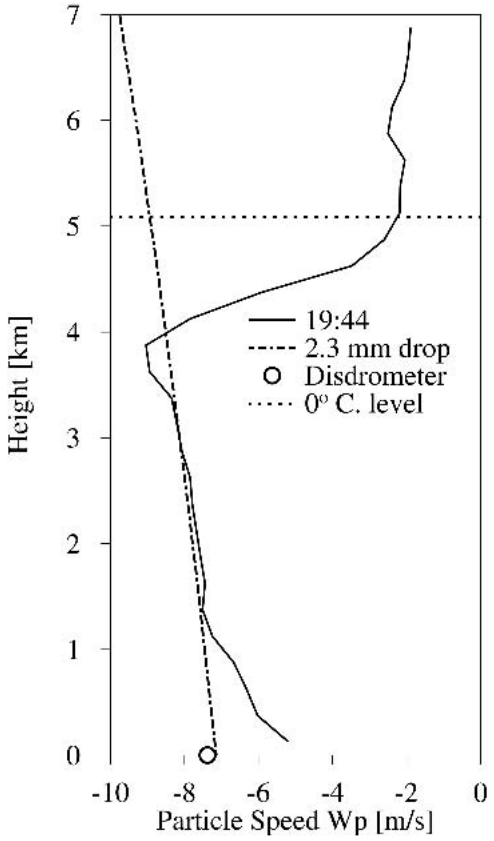

FIG. 7. Particle fall speeds derived by EVAD analysis of radar volume scan data, commencing at 1944 LT on 25 Oct 1990 (solid line). The dash–dot line is the fall speed profile for a raindrop of 2.3-mm diameter. Corrected for a vertical airspeed of 0.3–0.7 m s^{-1} the corrected drop diameter of 2.5 mm is close to the derived fall speed value for distrometer data (○).

was representative of a warmer air mass. Radar data were collected at elevation angles of 7°, 9°, 11°, 13°, 15°, 17.5°, and 20°. Figure 9 indicates the fall speed profile derived from the volume scan taken at 2329 eastern daylight time (EDT; UTC − 4 h). When downward vertical airspeeds of 0.3 m s^{-1} are removed, the fall speed profile was closer to that of a raindrop of 2.2-mm diameter. For this case there is a larger uncertainty in the derived fall speed values because the EVAD regression is applied over a smaller range of elevation angles. However, there is no first-order trend in fall speeds below 3 km. A look at the VAD-derived vertical speeds (not shown) indicates highly consistent variations in fall speed with height among the various elevation angles in the lowest 1.5 km and just below the melting level. The vertical airspeeds are very slow, so no strong convergence is taking place. Further aggregation in the melting layer is possible resulting in anomalously fast fall speeds just below the melting layer, as in the 25 October case at Penang.

Steady rain fell from 2325 to 2340 EDT, the period chosen for averaging disdrometer data for calculation of a derived mean fall speed. This speed is indicated in Fig. 9 as an open circle. There is a general consistency to the first order with the radar fall speed profile.

Figure 10 shows the velocity moment for a scan performed at 2323 EDT in a vertically pointing configuration. Velocities correspond to precipitation fall speeds and the range to height above ground. The sample volume is quite small and the fall speed values are adversely affected by very low reflectivity values in the lowest 2 km, the range associated with the lowest signal quality index (SQI). The transition to faster fall speeds in the melting layer is obvious. However, in contrast to the EVAD analysis, there is no indication of anomalously high fall speeds just below the melting layer. Inspection of the sweep data velocities and intensities reveals that an area of higher reflectivities passed by to the south of the radar. This area was included in the EVAD analysis and contained the larger drops responsible for the faster fall speeds. Thus, physical factors can account for significant sampling differences between the scanning strategies.

d. Toronto, 10 October 1991

Steady light rain with embedded heavier activity fell until 0930 EDT. Unlike the previous three cases, the

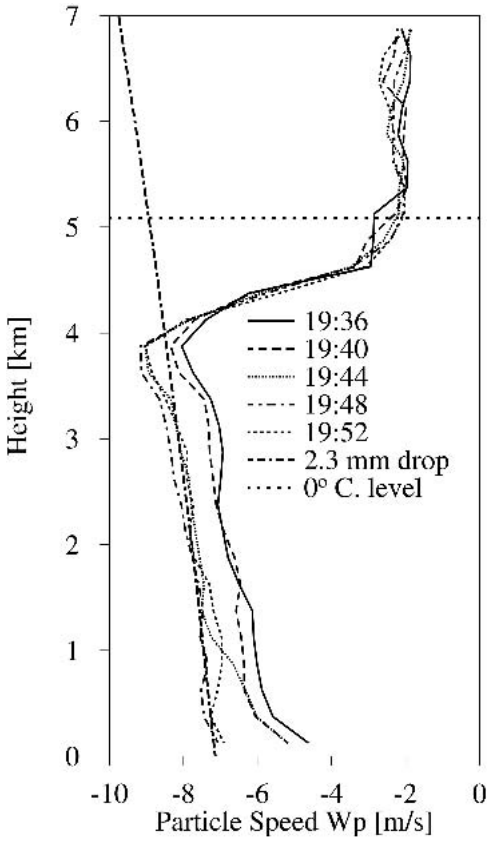

FIG. 8. Similar to Fig. 7 but for radar scans beginning at 1936 (solid), 1940 (dash), 1944 (dot), 1948 (dot–dash), and 1952 LT (short dash) on 25 Oct 1990.

Unauthenticated | Downloaded 12/08/22 09:02 PM UTC

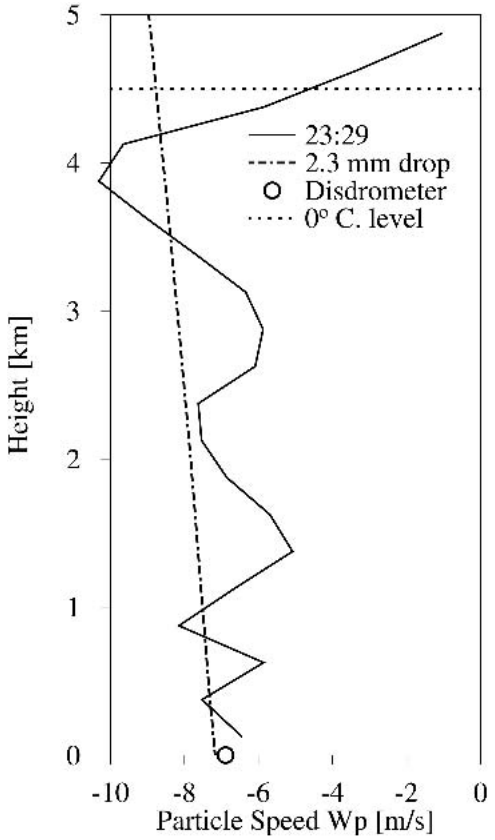

FIG. 9. Particle fall speeds derived by EVAD analysis of radar volume scan data commencing at 2329 EDT on 15 Jun 1991 (solid line). The dash–dot line is the fall speed profile for a raindrop of 2.3-mm diameter. The larger variability in fall speed values is due to EVAD regressions performed over a small range of elevation angles. The downdraft of 0.3 m s^{-1} is closer to the derived fall speed value for disdrometer data (○).

melting level was low at 2 km. Once again, sounding data from the Flint, Michigan, upper-air station were used in the EVAD analysis as Buffalo was in the warm sector. Radar data were collected at 15 elevation angles from 5° to 75°. Figure 11 shows the fall speed profile from the EVAD analysis of the radar volume scan data taken at 0850 EDT. When derived downward air speeds of 1.0 m s^{-1} were removed, the fall speed profile is closer to that of a raindrop of 1.5-mm diameter. There is no indication of anomalously large fall speeds just below the melting level, instead the fall speeds are quite low. There is, in fact, a trend to higher fall speeds at lower levels. In this case, it appears that a horizontal sampling bias is responsible for this apparent trend. In the individual elevation angle data, areas of higher reflectivities are apparent toward the western (upwind) direction. These areas contain the larger drops that have not been advected far enough in the horizontal to be detected by the high-elevation angle scans at higher heights.

The disdrometer data indicated particularly steady rain conditions from 0850 to 0905 EDT. Thus, this period was used to average drop spectra. The resultant mean-derived fall speed is indicated in Fig. 11 as an open circle. Both this value and the one from the EVAD analysis just below the melting layer are quite consistent. This further indicates insignificant raindrop spectra evolution due to drop collision at this low rain rate, and that the increase in fall speeds toward the ground is due to advective or sampling effects. Unlike the other three cases, smaller ice particles that melt into smaller raindrops are developed in this cold temperate environment.

e. Summary

The four cases examined all indicate signatures of RSDs undergoing negligible change with heights below the melting layer. Thus the raindrop spectra at ground level are not only representative of the spectra below the bright band, but often are fingerprints of the snowflake distribution above the melting layer. This is also suggested by Zawadzki et al. (1994) and supported by Thomson and List (1996).

Furthermore, the reflectivity-weighted mean diameters (D_{ref}) of the drop spectra are positively correlated with the rain rate (R). The regression equation relating these two parameters for the four cases is given by $D_{ref} = 0.43\ R + 1.24$ and applies to a rainfall range of 1–3 mm h^{-1}.

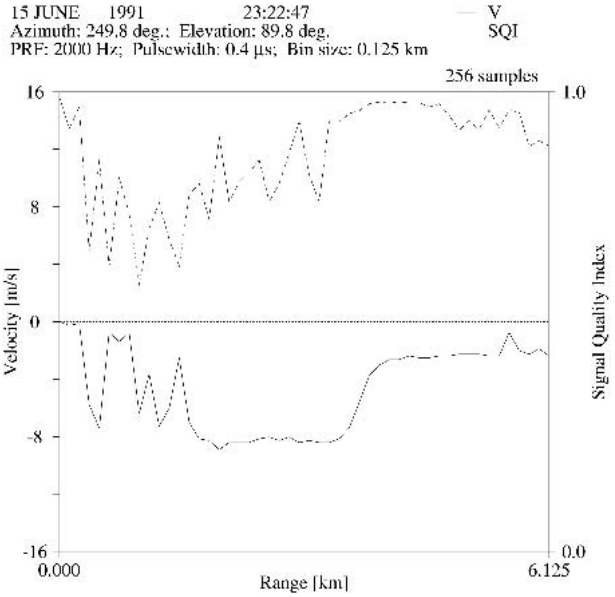

FIG. 10. Fall speed (solid line) and SQI (dashed line) as a function of range (height) for a vertically pointing radar scan acquired at 2322 EDT on 15 Jun 1991. Very weak reflectivities affect values below 2 km height. The SQI is the ratio of 1st lag to 0th lag Doppler autocorrelation.

Unauthenticated | Downloaded 12/08/22 09:02 PM UTC

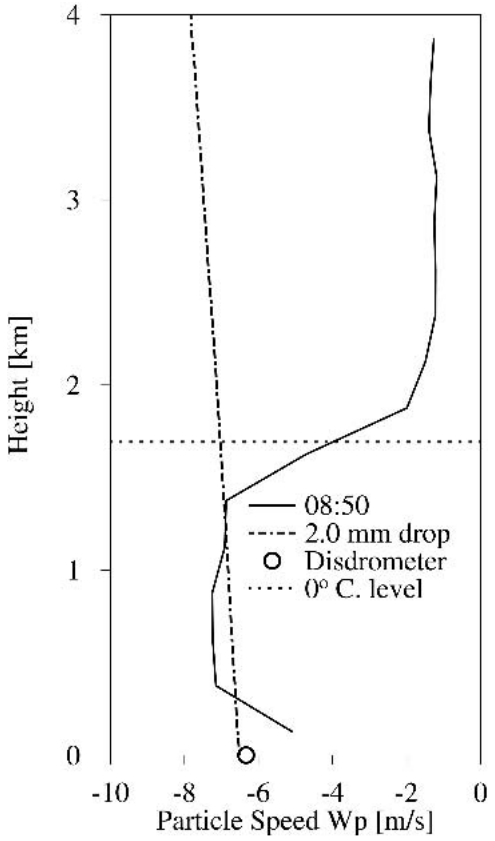

FIG. 11. Particle fall speeds derived by EVAD analysis of radar volume scan data commencing at 0850 EDT on 10 Oct 1991 (solid line). The dash–dot line is the fall speed profile for a raindrop of 2.0-mm diameter. The derived fall speed value for disdrometer data (○) is also included. With a downdraft of 1 m s^{-1} the drop diameter is 1.5 mm, i.e., much lower than the extrapolated value and the disdrometer point.

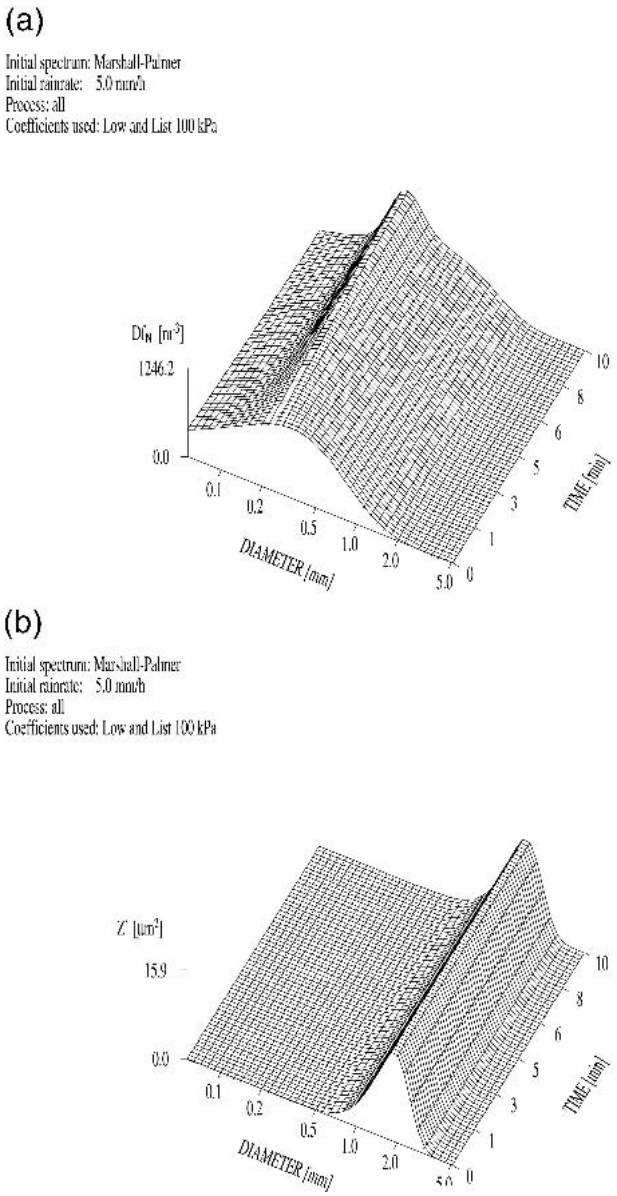

FIG. 12. Modeled evolution of raindrop spectra from a Marshall–Palmer (1948) distribution of rain rate 5 mm h^{-1} in (a) number concentration per logarithmic diameter interval and (b) derived reflectivity per diameter interval representations.

4. The evolution of raindrop spectra to equilibrium

List et al. (1987) have postulated that all rain in a shaft evolves to an equilibrium spectrum of unique shape no matter what the rain rate. Contrary to this finding, the measured spectra, represented by their radar reflectivity–weighted diameters for rain rates <5 mm h^{-1}, actually remain constant between the melting layer and the ground. This apparent discrepancy is investigated using a drop collision numerical model starting with Marshall–Palmer distributions with the parameterization in Low and List (1982a,b; with corrections in List et al. 1987). With the assumptions of an average fall speed for 2.4-mm drops of 7 m s^{-1}, a melting layer at ~4200 m (for the Malaysian case), and a constant pressure of 100 kPa, the travel time between the bottom of the melting layer and the ground would be ~10 min. The results are presented in Figs. 12a and 12b. It is seen from both representations that not much of a change in original distribution is expected for both initial distributions. Thus it can be argued that it is the lack of evolution at low rain rates that limits the change in spectra. This is consistent with the discussions on spectral evolution by McFarquhar and List (1991) and Srivastava (1988).

5. Summary and conclusions

Raindrop spectra can be characterized by a "Doppler-mean" drop size diameter that is based on a specific Doppler-mean velocity. Doppler-mean raindrop size

Unauthenticated | Downloaded 12/08/22 09:02 PM UTC

profiles for four cases were obtained after corrections for upward air velocity by the extended Velocity Azimuth Display (EVAD) method. Two independent measuring systems were applied for checking the Doppler radar–derived spectra: a Joss–Waldvogel disdrometer at the ground and a PMS 2-DP laser probe mounted on an aircraft. State parameters were established by ground measurements, radiosondes, and aircraft.

The conclusions of the studies are as follows.

1) The vertical profiles of the mean fall velocity of raindrops in cold rain processes of steady nonconvective clouds for an equatorial location (Penang, Malaysia) and a midlatitude site (Toronto, Canada) are similar for light-to-moderate rain rates.
2) When corrected for pressure, the resulting fall speed profiles can be compared with those for drops of constant, case-specific sizes with a diameter range of 1.5 to 2.5 mm. This suggests that the spectrum evolution is negligible at low-to-moderate rain rates because the drop interaction rate is too low to approach equilibrium on the fall to the ground.
3) Raindrop fall speed profiles, based on reflectivity-weighted mean fall speeds established from EVAD analyses of radar data, agreed well with derived values from a Joss–Waldvogel disdrometer at the ground and an airborne PMS 2-DP laser spectrometer.
4) For the four cases presented, larger Doppler-mean drop diameters are associated with higher rain rates.
5) Weighted raindrop diameter profiles, taken at 4-min intervals from radar scans, may be sensitive to advection of different drop spectra as well as the sampling bias of the radar scan.
6) The observations suggest that when ice crystals of large mass melt into large raindrops, the fall speed profile shows a noticeable anomaly constrained to within 500 m below the melting layer. This feature is not present when fall speed profiles have slower values. The anomaly appears to be due to the presence of a few very large raindrops more prone to rapid breakup in collision with smaller drops.

It would be advantageous to extend these studies to nonconvective rainfall of higher intensity.

Acknowledgments. The Joint Malaysian Rain Project was funded by the Malaysian Meteorological Service and the National Sciences and Engineering Research Council of Canada. The project was made possible in the first place by a seed grant by Professor G. Connell, president of the University of Toronto. Particular support was provided by Datuk Amar Stephen Yong, minister for Science and Technology of Malaysia; Dr. Jingjai Hanchanlash, director of the Canadian International Development and Research Center, Singapore Office; and Mr. P. Markandan, director-general of the Malaysian Meteorological Service. The present study heavily relies on part of the Ph.D. thesis of Nissen (1996).

REFERENCES

Atlas, D., 1964: Advances in radar meteorology. *Advances in Geophysics,* Vol. 10, Academic Press, 317–478.

——, R. C. Srivastava, and R. S. Sekron, 1973: Doppler radar characteristics of precipitation at vertical incidence. *Rev. Geophys. Space Phys.,* **11,** 1–35.

Battan, L. J., and J. B. Theiss, 1966: Observations of vertical motions and particle sizes in a thunderstorm. *J. Atmos. Sci.,* **23,** 78–87.

Beard, K. V., 1976: Terminal velocity and shape of cloud and precipitation drops aloft. *J. Atmos. Sci.,* **33,** 851–864.

Caton, P. G. F., 1966: Raindrop size distribution in the free atmosphere. *Quart. J. Roy. Meteor. Soc.,* **92,** 15–30.

Cifelli, R., C. R. Williams, D. K. Rajopadhyaya, and S. K. Avery, 2000: Drop-size distribution characteristics in tropical mesoscale convective systems. *J. Appl. Meteor.,* **39,** 760–777.

Doviak, R. J., and D. S. Zrnić, 1984: *Doppler Radar and Weather Observations.* Academic Press, 458 pp.

Gossard, E. E., and R. G. Strauch, 1983: *Radar Observation of Clear Air and Clouds.* Elsevier, 280 pp.

——, ——, and R. R. Rogers, 1990: Evolution of dropsize distributions in liquid precipitation observed by ground-based Doppler radar. *J. Atmos. Oceanic Technol.,* **7,** 815–828.

Joss, J., and A. Waldvogel, 1967: Ein Spektrograph für Niederschlagstropfen mit automatischer Auswertung. *Pure Appl. Geophys.,* **68,** 240–246.

Lhermitte, R. M., and D. Atlas, 1961: Precipitation motion by pulse-Doppler radar. *Proc. Ninth Conf. on Radar Meteorology,* Kansas City, KS, Amer. Meteor. Soc., 218–223.

List, R., N. R. Donaldson, and R. E. Stewart, 1987: Temporal evolution of drop spectra to collisional equilibrium in steady and pulsating rain. *J. Atmos. Sci.,* **44,** 362–372.

——, R. Nissen, G. M. McFarquhar, D. Hudak, N. P. Tung, T. S. Kang, and S. K. Soo, 1991: Properties of tropical rain. Preprints, *25th Int. Conf. on Radar Meteorology,* Paris, France, Amer. Meteor. Soc., 774–777.

Low, T. B., and R. List, 1982a: Collision, coalescence and breakup of raindrops. Part I: Experimentally established coalescence efficiencies and fragment size distributions in breakup. *J. Atmos. Sci.,* **39,** 1591–1606.

——, and ——, 1982b: Collision, coalescence and breakup of raindrops. Part II: Parameterization of fragment size distributions. *J. Atmos. Sci.,* **39,** 1607–1619.

Marshall, J. S., and W. M. Palmer, 1948: The distribution of raindrops with size. *J. Meteor.,* **5,** 165–166.

Matejka, T., and R. C. Srivastava, 1991: An improved version of the extended velocity-azimuth display analysis of single-Doppler radar data. *J. Atmos. Oceanic Technol.,* **8,** 453–466.

McFarquhar, G. M., and R. List, 1991: The raindrop mean free path and collision rate dependence on rainrate for three-peak equilibrium and Marshall–Palmer distributions. *J. Atmos. Sci.,* **48,** 1999–2003.

——, and ——, 1993: The effect of curve fits for the disdrometer calibration on raindrop spectra, rainfall rate, and radar reflectivity. *J. Appl. Meteor.,* **32,** 774–782.

——, ——, D. Hudak, R. Nissen, J. S. Dobbie, N. P. Tung, and T. S. Kang, 1996: Flux measurements of pulsating rain with a disdrometer and Doppler radar during Phase II of the Joint Tropical Rain Experiment in Malaysia. *J. Appl. Meteor.,* **35,** 859–874.

Nissen, R., 1996: Effects of air pressure on raindrop size distributions: Modelling and field data verification. Ph.D. thesis, Department of Physics, University of Toronto, 140 pp.

Probert-Jones, J. R., and W. G. Harper, 1961: Vertical air motion in showers as revealed by Doppler radar. *Proc. Ninth Weather Radar Conf.,* Kansas City, MO, Amer. Meteor. Soc., 225–232.

Unauthenticated | Downloaded 12/08/22 09:02 PM UTC

Rogers, R. R., 1964: An extension of the Z-R relation for Doppler radar. *Proc. 11th Weather Radar Conf.,* Boulder, CO, Amer. Meteor. Soc., 158–161.

Seliga, T. A., and V. N. Bringi, 1976: Potential use of radar differential reflectivity measurements at orthogonal polarizations for measuring precipitation. *J. Appl. Meteor.,* **15,** 69–76.

Srivastava, R. C., 1988: On the scaling equations governing the evolution of raindrop size distributions. *J. Atmos. Sci.,* **45,** 1091–1092.

——, T. J. Matejka, and T. J. Lorello, 1986: Doppler radar study of the trailing anvil region associated with a squall line. *J. Atmos. Sci.,* **43,** 356–377.

Thomson, A. D., and R. List, 1996: Raindrop spectra and updraft determination by combining Doppler radar and disdrometer. *J. Atmos. Oceanic Technol.,* **13,** 465–476.

Zawadzki, I. I., E. Monteiro, and F. Fabry, 1994: The development of drop size distributions in light rain. *J. Atmos. Sci.,* **51,** 1100–1113.

Unauthenticated | Downloaded 12/08/22 09:02 PM UTC